CrystEngComm

ROYAL SOCIETY OF CHEMISTRY

COMMUNICATION

View Article Online
View Journal | View Issue

Cite this: *CrystEngComm*, 2023, **25**, 2353

Received 10th February 2023,
Accepted 19th March 2023

DOI: 10.1039/d3ce00138e

rsc.li/crystengcomm

(*Z*)-4,4′-Stilbene dicarboxylic acid, the overlooked metal–organic framework linker†

Lucy R. Hunter, *[a] Joshua K. G. Karlsson, [a] Jonathan D. Sellars [b] and Michael R. Probert *[a]

Metal–organic frameworks exhibit a broad and diverse structural portfolio, with rational structural engineering of frameworks becoming increasingly desirable. Fine-tuning the metal–ligand combination offers a simple way to adjust a framework's physical and chemical properties. One route to synthesising frameworks with new physical properties and topologies without altering the chemical composition is through the use of ligand isomers. Whilst *trans*-stilbene derivatives, such as (*E*)-4,4′-stilbene dicarboxylic acid have been exhaustively studied producing numerous unique frameworks, its ligand-originated isomer, *cis*-stilbene derivative (*Z*)-4,4′-stilbene dicarboxylic acid has not. Herein, we describe the synthesis of ten lanthanide (*Z*)-4,4′-stilbene dicarboxylic acid frameworks, five possessing non-interpenetrating 2D sheet structures and five microporous 3D frameworks with 1-dimensional pore channels that incorporate internal voids of up to 5.2 Å in diameter. These three-dimensional frameworks have a hitherto unrecognised underlying net topology, now registered as lmj1.

1. Introduction

Since reticular chemistry was introduced as a concept, Metal–Organic Frameworks (MOFs) have emerged as one of the most abundant and investigated classes of porous crystalline material in the 21st century.[1,2] MOFs are highly ordered crystalline networks that give rise to many desirable and interesting properties, such as permanent porosity, thermal stability and structural versatility.[3–5] Consequently, they have found many applications with examples as gas storage materials,[6–8] catalysts,[9,10] molecular sensors,[11–13] for drug encapsulation and as carrier vehicles.[14,15]

The ability of a MOF to carry out such applications depends on several factors, for example, the size and shape of a pore, metal node connectivity and the inclusion of different surface functional groups.[16] Extensive efforts focus on advancing and optimising a framework's function by virtue of changing the above features, with one strategy examining framework isomers.[17,18] Examples of framework isomers include interpenetrated isomers,[19] secondary building unit (SBU) isomers,[20] orientation isomers,[21] solvent-based isomers[22] and ligand-originated isomers. Of these, ligand-originated isomers are compelling as they create an avenue for synthesising new porous scaffolds and enable the physical behaviour of a MOF to be modified without changing the MOF composition. A recent example of this by He and co-workers varies the position of a methyl group on the diisophthalate linkers to create three unique frameworks with varying abilities to uptake and store a range of gases.[23] In addition to positional modifications, orientation isomers such as those containing *E*/Z functionality or chiral centres are also possible. When initial frameworks were engineered, strong, rigid linear linkers were employed to design the most robust scaffolds, (*E*)-4,4′-stilbene dicarboxylic acid ((*E*)-H_2SDC) is one example that has been extensively studied.[24–26] These frameworks have displayed a diverse array of properties from variable temperature magnetism to high levels of luminescence,[25] however, the ligand isomer (*Z*)-4,4′-stilbene dicarboxylic acid ((*Z*)-H_2SDC) remains to be studied in any detail.[27–29]

Herein, we report the synthesis and crystal structures of ten metal–organic frameworks derived from (*Z*)-H_2SDC and lanthanide metals. From this, we have produced five 2D sheet and five microporous 3D frameworks which incorporate internal voids of 5.2 Å and demonstrate a new underlying net topology.

[a] *School of Natural and Environmental Sciences, Newcastle University Faculty of Science Agriculture and Engineering, Newcastle upon Tyne, UK.*
E-mail: l.hunter6@newcastle.ac.uk, michael.probert@newcastle.ac.uk
[b] *Newcastle University Faculty of Medical Sciences, Newcastle upon Tyne, UK*

† Electronic supplementary information (ESI) available: Contains crystallographic information file data, IR, TGA and DSC, PXRD patterns, fluorescence excitation wavelengths, raw excitation data and luminescence spectra. All structures are submitted to the CSD and can be found under deposition numbers 2088043–2088050, 2088053, and 2088056. For ESI and crystallographic data in CIF or other electronic format see DOI: **https://doi.org/10.1039/d3ce00138e**

2. Materials and methods

2.1 General remarks

(*Z*)-4,4′-Stilbene dicarboxylic acid, *N*,*N*-dimethylformamide (DMF) and all lanthanide salts were used as supplied unless otherwise stated. For synthesis, a solution of (*Z*)-H_2SDC and 1.2 equivalents of $LnCl_3$ were heated at 80 °C for 48 h before leaving to evaporate over 4–16 weeks slowly. 10 high quality crystals were produced. Five 2D coordination polymers (CP) with Sm (**1**), Eu (**2**), Gd (**3**), Tb (**4**) and Ho (**5**) and five 3D frameworks, Eu (**6**), Gd (**7**), Tb (**8**), Ho (**9**) and Er (**10**). Further details of synthesis can be found in the ESI.†

3. Crystal structure analysis

Lanthanides are often used to create large secondary building units due to their spacious coordination sphere and ability to create multiple bonds with carboxylic acid linkers. This leads to the creation of diverse topologies, as is observed herein. Crystal structures **1–5** demonstrate closed 2D non-interpenetrating sheet frameworks that are all isostructural. The structures are constrained to a triclinic system in the $P\bar{1}$ space group presenting no higher symmetry. Each asymmetric unit contains two crystallographically independent bridged lanthanide(III) metals, with both lanthanide centres having a coordination geometry of eight, leading to dodecahedral polyhedral centres (Fig. 1a). Each centre is coordinated to five (*Z*)-4,4′-stilbene carboxylate ((*Z*)-SDC) ligands and two water molecules. Four of these ligands are directly coordinated to another lanthanide centre in a bidentate bridging mode creating a 1-dimensional inorganic chain extending parallel to the unit cell *a*-axis. (Fig. 1b). The fifth linker within the coordination sphere binds in a bidentate chelating mode. Ligand pairs bridging the 1D organic chain form an alternating pattern. One pair of ligands pillar the 1D chains along the *c*-axis, and the next pair in the chain bind only *via* one terminal carboxylate of the linker whilst a carboxylic acid caps the sheet structure in the *b*-direction (Fig. 1c), preventing 3D framework formation due to a hydrogen atom still being present. These free carboxylic acids face each other between the 2D layers, with the nearest free neighbour lying only 5.481 Å apart. The average metal–metal (M–M) distance along the 1D inorganic chain is 4.86 Å. The alkene torsion angles of the four linkers in the formula unit range between ~1.3 and 7.4°. The benzene rings sit out of plane with twist angles between ~63.7–110.3°. When viewing the sheet structure in the ac plane you can see the compact nature of the 2D sheet framework (Fig. 1d). Topological analysis has been undertaken to reveal all complexes **1–5** possess the bey (3,4-c) underlying net topology representing less than 2% of MOFs submitted to the CSD.[30]

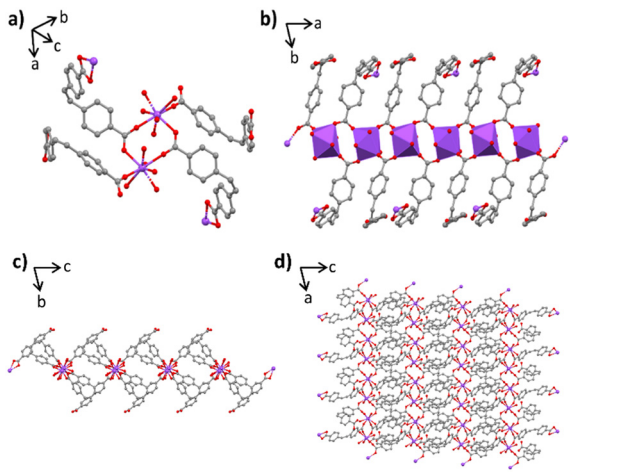

Fig. 1 Four representations of frameworks 1–5 (lanthanide – purple, C – grey, O – red); a) formula unit contents of complexes **1–5**; b) 1D inorganic chain representation of frameworks **1–5** including inorganic polyhedral representation; c) extended visual representation of CPs **1–5** when viewing down the *a*-axis; d) extended visual representation of the sheet nature of CPs **1–5** when viewed down the *b*-axis. Hydrogen atoms and guest solvent molecules excluded for clarity.

Alongside this, the remaining complexes **6–10** also crystallise in the $P\bar{1}$ space group and are 3D non-interpenetrated frameworks with 1D channel pores dispersed throughout their structure. Solvent accessible voids occupy 5.9% of the unit cell volume, 176 $Å^3$ with a 1.0 Å probe radius, calculated using Mercury (2020.3). When solvent molecules are removed from the pores the accessible volume is increased to 219.58 $Å^3$, 7.4% of the unit cell volume with a 1.0 Å probe radius. The largest accessible spherical void is 5.2 Å diameter when solvent has been removed, making these frameworks microporous. Thermogravimetric analysis (TGA) suggests there are three free solvent molecules per asymmetric unit in the void space of the pristine samples of **6–10** (Fig. S12†). The coordination number observed for the metal centres in the 2D frameworks persist in the 3D structures. Similarities recur with 3D frameworks also containing two crystallographically independent lanthanide(III) metal centres (Fig. 2a). On closer inspection, one metal centre resembles the exact coordination sphere observed in complexes **1–5**, with lanthanides directly coordinated to three ligands and two water molecules to create the 1D backbone along the *c*-axis. Whilst the other lanthanide centre possesses a DMF molecule in place of a water molecule in its coordination sphere, that creates a bridged lanthanide pair sitting independently from the 1D inorganic chain (Fig. 2b). The M–M distance between bridged lanthanides ranges between ~4.89–4.98 Å, the M–M distance for the isolated metal pairs is slightly longer at 5.07 Å. The torsion angles for the formula unit's three (*Z*)-SDC linkers differ slightly with alkene torsion angles ranging between ~2.8° and 7.7°. The rings do not sit planar to one another and have varying twist angles between ~72.4° and 114.3°. The crystal structures of the isolated (*Z*)-H_2SDC and *cis*-stilbene components have not been published to date, with crystallisation attempts not resulting in samples of suitable quality for analysis. A comparison between the free linker and complexed linker is therefore not possible, but the crystallisation of these

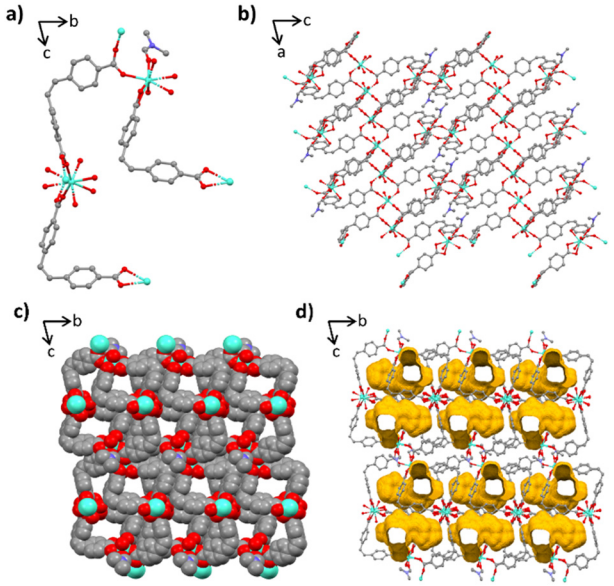

Fig. 2 Four representations of frameworks **6–10** (lanthanide – green, C – grey, O – red, N – blue); a) formula unit of complexes **6–10**, showing the two crystallographic independent metal centres; b) extended representation of the frameworks viewed down the *b*-axis; c) space-filing model of frameworks **6–10**, viewed down the *a*-axis; d) frameworks viewed down the *a*-axis, solvent accessible void space is modelled in yellow. Hydrogen atoms and guest molecules excluded for clarity.

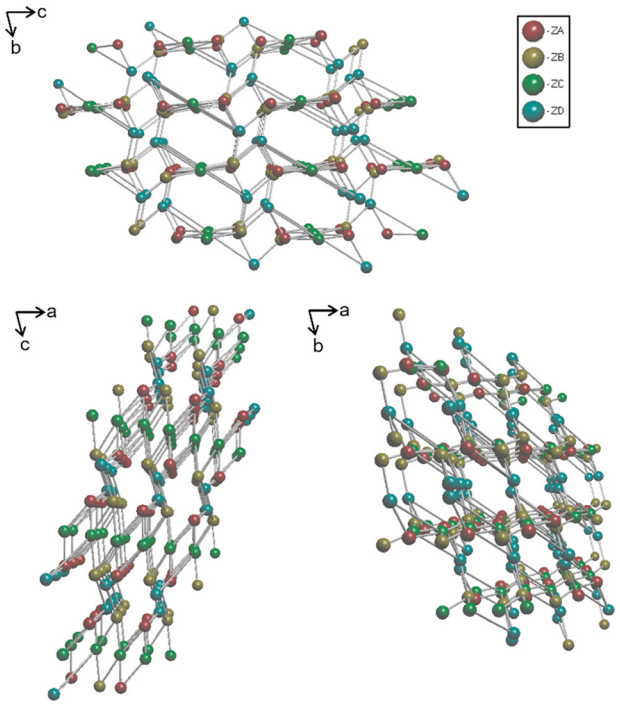

Fig. 3 Simplified underlying net representations of frameworks **6–10** viewed separately down all three crystallographic axes. The red sphere (ZA) represents the 3-c node, the yellow/brown sphere (ZB) is a 4-c node, green spheres show (ZC) are 5-c nodes, and finally blue spheres (ZD) are 4-c nodes.

frameworks gives additional experimental insight into how the rings sit relative to one another supporting numerous quantum chemical computational studies.[31,32]

Topological analysis reveals that complexes **6–10** have a previously unreported underlying net topology. Frameworks **6–10** have complicated underlying symmetry, comprising a 4-nodal with (3-c)(4-c)(4-c)(5-c) connectivity, and TD10 value of 791. The lanthanide backbone creates a series of 4-c rings extending along the *a*-axis represented by nodes ZB and ZD, whilst ZA and ZC represent the 3-c and 5-c nodes respectively (Fig. 3). The seemingly complicated nature of the underlying net stems from the use of unconventional non-linear (*Z*)-SDC linkers, combined with the two crystallographically independent lanthanide metal centres. Organic linkers were once sought to be linear and rigid, the increasing popularity of the use of non-linear linkers, such as (*Z*)-4,4′-stilbene dicarboxylic acid. The use of non-linear linkers can result in new structures that are becoming increasingly unpredictable, but this has led to an increase in newfound topologies.[33] The new net representation reported herein has been registered as **lmj1**.

4. Rate-determined dimensionality

A particularly interesting feature of our systems occurs on leaving 2D crystals in mother liquor solution for extended periods. When left for >30 days, we observe the exclusive formation of 3D framework crystals within the same vial. PXRD data obtained in the intermediate time between exclusive 2D and 3D formation displays a pattern containing peaks correlating to a mixture of the individual components (Fig. S23†). Unsurprisingly, there are similarities between the 2D and 3D frameworks, suggesting the 3D framework is the product of modification to the existing 2D framework. Both 2D and 3D scaffolds contain the same 1D inorganic backbone, while 3D frameworks also incorporate another crystallographically independent metal centre, this can be best visualised when viewing both sets of frameworks in the (010) plane (Fig. 4).

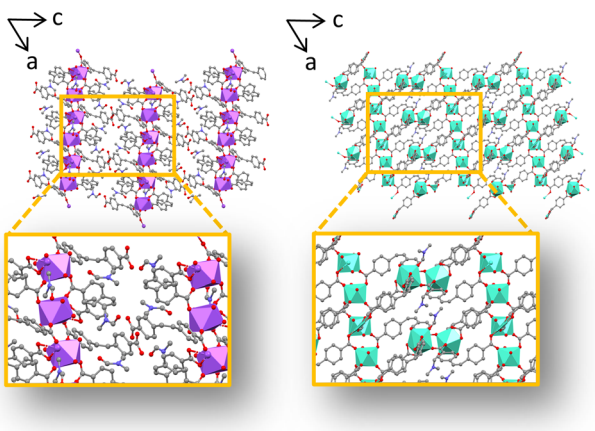

Fig. 4 Representation of frameworks **1–5** (left) and **6–10** (right) both viewed down the crystallographic *b*-axis. The inorganic chain has been highlighted in both images to show the similarities between the two sets of framework.

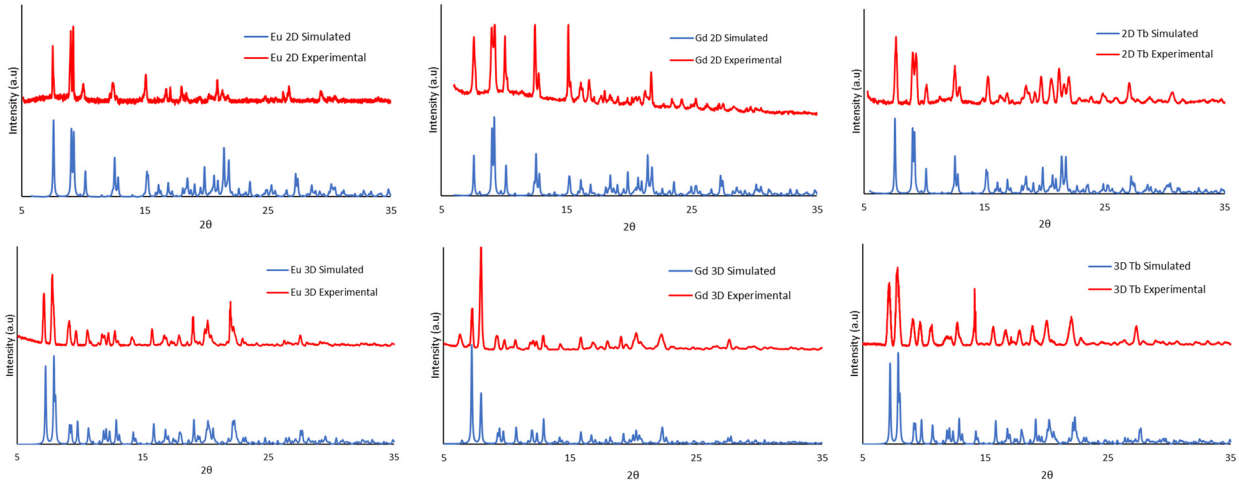

Fig. 5 Top: PXRD patterns of the 2D Eu, Gd, and Tb frameworks bulk material. Bottom: PXRD patterns of 3D Eu, Gd, and Tb frameworks bulk material. Blue – simulated powder patterns from single crystal data. Red – experimental data. Data was collected using a Rigaku XtaLAB Synergy, CuKα (λ = 1.5406 Å) radiation source with reduced beam divergence, data scaled to the most intense peak.

It is believed that the free carboxylic acids in the 2D framework undertake further complexation over the extended reaction time. This result suggests that the formation of 2D frameworks is under kinetic control whilst the 3D frameworks are formed as the thermodynamic product seen as an artefact of the slow crystallisation method. For two out of our ten frameworks, no transformation between 2D and 3D was observed. At either end of the series, the 3D samarium analogue has not been isolated, whilst neither has the 2D erbium analogue. Like many lanthanide frameworks synthesised, the structural limitations are expected to be a consequence of the atomic size difference across the series.

5. Luminescence studies

It has been established that stilbene MOFs show interesting luminescence properties,[24–26] in particular, stilbene emission profiles can be prone to changes in luminescence with ligand orientation. For example, in the luminescence spectra for 2D and 3D zinc (*E*)-stilbene dicarboxylic acid MOF isomers, a significant energy shift and peak shape difference is observed, due to ligand–ligand charge transfer coupling between co-facial and closely related stilbene units in space.[24]

Not only this, it has been shown that lanthanide MOFs, namely Sm, Eu, Gd, Tb and Dy analogous, are able to behave as small ion and/or solvent sensors, using ligand chromophores to absorb light and displaying an antenna effect to the lanthanide metal, emitting in the visible and UV region.[34] The highest emission intensity and colour purity is observed with Eu and Tb, with the luminescence profiles being enhanced or quenched with the absorption of small molecules or ions.[35]

Consequently, we decided to investigate the solid-state luminescent properties of our Eu, Gd and Tb frameworks, whereby we have structural data for both 2D and 3D analogues for comparison.

To ensure compound purity, PXRD of the bulk samples were conducted (Fig. 5). The PXRD patterns of the bulk samples show clear phase purity and highlight that 2D and 3D frameworks can be isolated separately. Upon studying our frameworks luminescence profiles, they all showed ligand-based luminescence emitting in the blue region of the electromagnetic spectrum with the peak maxima at 450 nm attributed to π–π* transitions in the highly conjugated linker. The emission profile is comparable to the free (*Z*)-H_2SDC linker, with the same peak maxima and featureless profile (Fig. S24†).

The emission intensity of all frameworks was considerable, this is likely due to the isolation and rigidification of chromophores once complexed, a phenomenon reported for *trans*-MOF analogues.[25]

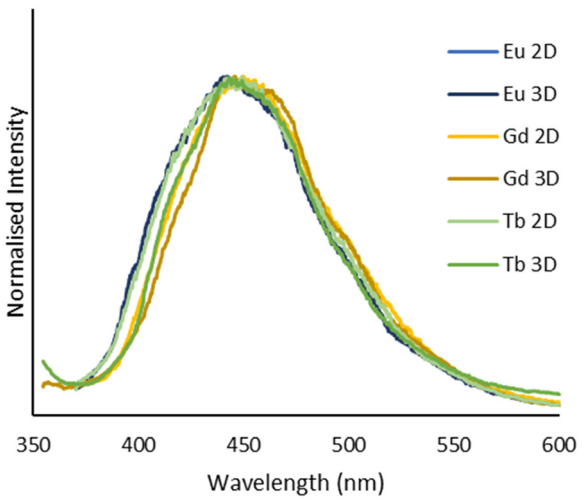

Fig. 6 Luminescence profiles of compounds **2**–**4** and **6**–**8**: a comparison of both 2D and 3D frameworks emission spectra for Eu, Gd, and Tb, all displaying ligand-based emission. Recorded at room temperature using a Hitatchi F-4500 spectrophotometer.

There appear to be no discernible differences between the 2D and 3D luminescence spectra, with all frameworks emitting the same profile. As aforementioned, frameworks **2–4** and **6–8** were studied as their independent metal ions emit in the UV-visible light region. We observed no sharp discrete emission intensity from any frameworks studied, suggesting the antenna effect from the chromophoric linker to the metal ions does not occur due to a large energy separation between the HOMO and LUMO (Fig. 6).

6. Conclusion

We have demonstrated the successful synthesis of a class of new metal–organic frameworks based around the previously unstudied (*Z*)-4,4′-stilbene dicarboxylic acid. We have synthesised ten related frameworks, of which five are 2D sheet frameworks, and five are 3D microporous frameworks with a void space of up to 5.2 Å and possess a newly discovered underlying net topology, **lmj1**. The 2D frameworks isolated are a structural intermediate to the 3D frameworks transforming over extended periods of time. Luminescence emission shows frameworks emit a large proportion of ligand-based luminescence with a peak maxima of 450 nm and a profile comparable to the free linker.

Conflicts of interest

There are no conflicts of interest to declare.

Acknowledgements

The authors wish to thank Newcastle University's School of Natural and Environmental Sciences for funding the work and thank Dr Onoriode Esegbue for collecting TGA and DSC data.

Notes and references

1 H. Li, M. Eddaoudi, M. O'Keeffe and O. M. Yahgi, *Nature*, 1999, **402**, 276–279.
2 N. W. Ockwig, O. Delgado-Friedrichs, M. O'Keeffe and O. M. Yaghi, *Acc. Chem. Res.*, 2005, **38**, 176–182.
3 O. K. Farha and J. T. Hupp, *Acc. Chem. Res.*, 2010, **43**, 1166–1175.
4 L. Z. Cai, X. M. Jiang, Z. J. Zhang, P. Y. Guo, A. P. Jin, M. S. Wang and G. C. Guo, *Inorg. Chem.*, 2017, **56**, 1036–1040.
5 A. Michaelides, S. Skoulika and M. G. Siskos, *CrystEngComm*, 2008, **10**, 817–820.
6 O. K. Farha, A. Ö. Yazaydin, I. Eryazici, C. D. Malliakas, B. G. Hauser, M. G. Kanatzidis, S. T. Nguyen, R. Q. Snurr and J. T. Hupp, *Nat. Chem.*, 2010, **2**, 944–948.
7 D. Alezi, Y. Belmabkhout, M. Suyetin, P. M. Bhatt, L. J. Weseliński, V. Solovyeva, K. Adil, I. Spanopoulos, P. N. Trikalitis, A. H. Emwas and M. Eddaoudi, *J. Am. Chem. Soc.*, 2015, **137**, 13308–13318.
8 D. Alezi, Y. Belmabkhout, M. Suyetin, P. M. Bhatt, L. J. Weseliński, V. Solovyeva, K. Adil, I. Spanopoulos, P. N. Trikalitis, A. H. Emwas and M. Eddaoudi, *J. Am. Chem. Soc.*, 2015, **137**, 13308–13318.
9 J. Lee, O. K. Farha, J. Roberts, K. A. Scheidt, S. T. Nguyen and J. T. Hupp, *Chem. Soc. Rev.*, 2009, **38**, 1450–1459.
10 S. Horike, M. Dincă, K. Tamaki and J. R. Long, *J. Am. Chem. Soc.*, 2008, **130**, 5854–5855.
11 L. E. Kreno, K. Leong, O. K. Farha, M. Allendorf, R. P. Van Duyne and J. T. Hupp, *Chem. Rev.*, 2012, **112**, 1105–1125.
12 A. Lan, K. Li, H. Wu, D. H. Olson, T. J. Emge, W. Ki, M. Hong and J. Li, *Angew. Chem., Int. Ed.*, 2009, **48**, 2334–2338.
13 A. Helal, H. L. Nguyen, A. Al-Ahmed, K. E. Cordova and Z. H. Yamani, *Inorg. Chem.*, 2019, **58**, 1738–1741.
14 H. Ding, L. Wu, T. Guo, Z. Zhang, B. M. Garba, G. Gao, S. He, W. Zhang, Y. Chen, Y. Lin, H. Liu, J. Anwar and J. Zhang, *Cryst. Growth Des.*, 2019, **19**, 3888–3894.
15 I. Abánades Lázaro and R. S. Forgan, *Coord. Chem. Rev.*, 2019, **380**, 230–259.
16 H. L. Jiang, Y. Tatsu, Z. H. Lu and Q. Xu, *J. Am. Chem. Soc.*, 2010, **132**, 5586–5587.
17 F. Guo, F. Wang, H. Yang, X. Zhang and J. Zhang, *Inorg. Chem.*, 2012, **51**, 9677–9682.
18 T. A. Makal, A. A. Yakovenko and H. C. Zhou, *J. Phys. Chem. Lett.*, 2011, **2**, 1682–1689.
19 L. Robison, X. Gong, A. M. Evans, F. A. Son, X. Wang, L. R. Redfern, M. C. Wasson, Z. H. Syed, Z. Chen, K. B. Idrees, T. Islamoglu, M. Delferro, W. R. Dichtel, F. X. Coudert, N. C. Gianneschi and O. K. Farha, *J. Am. Chem. Soc.*, 2021, **143**, 1503–1512.
20 L. Han, L. Qin, X. Z. Yan, L. P. Xu, J. Sun, L. Yu, H. B. Chen and X. Zou, *Cryst. Growth Des.*, 2013, **13**, 1807–1811.
21 L. Fan, K. Wang, K. Xu, Z. Liang, H. Wang, S. F. Zhou and G. Zhan, *Small*, 2020, **16**, 1–13.
22 A. Gheorghe, I. Imaz, J. I. Van Der Vlugt, D. Maspoch and S. Tanase, *Dalton Trans.*, 2019, **48**, 10043–10050.
23 M. He, Y. Wang, X. Gao, S. Li and Y. He, *Dalton Trans.*, 2018, **47**, 8983–8991.
24 C. A. Bauer, S. C. Jones, T. L. Kinnibrugh, P. Tongwa, R. A. Farrell, A. Vakil, T. V. Timofeeva, V. N. Khrustalev and M. D. Allendorf, *Dalton Trans.*, 2014, **43**, 2925–2935.
25 S. R. Mathis, S. T. Golafale, J. Bacsa, A. Steiner, C. W. Ingram, F. P. Doty, E. Auden and K. Hattar, *Dalton Trans.*, 2017, **46**, 491–500.
26 V. V. Semionova, E. M. Glebov, V. V. Korolev, S. A. Sapchenko, D. G. Samsonenko and V. P. Fedin, *Inorg. Chim. Acta*, 2014, **409**, 342–348.
27 J. Park, L. B. Sun, Y. P. Chen, Z. Perry and H. C. Zhou, *Angew. Chem., Int. Ed.*, 2014, **53**, 5842–5846.
28 Z. Wang, K. Müller, M. Valášek, S. Grosjean, S. Bräse, C. Wöll, M. Mayor and L. Heinke, *J. Phys. Chem. C*, 2018, **122**, 19044–19050.
29 L. Heinke, M. Cakici, M. Dommaschk, S. Grosjean, R. Herges, S. Bräse and C. Wöll, *ACS Nano*, 2014, **8**, 1463–1467.
30 *TopCryst*, **https://topcryst.com/i.php?show=d2981462-5f21-43f1-9512-df1ddd90b558&dbname=topcryst&topology=bey&ttdcode=800648&xrefcode=undefined**, (Accessed October 2022, version 2020.3).

31 D. Tzeli, G. Theodorakopoulos, I. D. Petsalakis, D. Ajami and J. Rebek, *J. Am. Chem. Soc.*, 2012, **134**(9), 4346–4354.
32 Y. Dou and R. E. Allen, *J. Chem. Phys*, 2003, **119**, 10658–10666.
33 D. Frahm, F. Hoffmann and M. Fröba, *CrystEngComm*, 2013, **15**, 9429–9436.
34 T. Gorai, W. Schmitt and T. Gunnlaugsson, *Dalton Trans.*, 2021, **50**, 770–784.
35 T. Wiwasuku, A. Chuaephon, U. Habarakada, J. Boonmak, T. Puangmali, F. Kielar, D. J. Harding and S. Youngme, *ACS Sustainable Chem. Eng.*, 2022, **10**, 2761–2771.

